Supporting Information

Pyridylarsine-based Cu(I) complexes showing TADF mixed with fast phosphorescence: speeding-up emission rate using arsine ligands

Alexander V. Artem'ev,[a]* Yan V. Demyanov,[a] Marianna I. Rakhmanova,[a] Irina Yu. Bagryanskaya[b]

[a]*Nikolaev Institute of Inorganic Chemistry, Siberian Branch of Russian Academy of Sciences, 3, Acad. Lavrentiev Ave., 630090 Novosibirsk, Russian Federation*
[b]*N. N. Vorozhtsov Novosibirsk Institute of Organic Chemistry, 9, Acad. Lavrentiev Ave., Novosibirsk 630090, Russian Federation*

*E-mail: chemisufarm@yandex.ru (Alexander V. Artem'ev)

Table of content

§1. Materials and Instrumentation

All synthetic procedures were carried out under an argon atmosphere using standard Schlenk technique. CuI (≥99%, Sigma), $[Cu(CH_3CN)_4]BF_4$ (≥99%, Acros), *n*-BuLi (2.5 M in hexanes, Sigma), 2-bromopyridine (≥99%, Acros), silica gel 60 (Macherey-Nagel, 60 Å pore size, 230-400 mesh) were used as purchased. CuCl (≥99%, Sigma) was additionally purified prior to use by subsequent washing with HCl_{aq}, water and acetone, followed by drying under vacuum. CuBr was freshly synthesized by treatment of $CuBr_2$ with Cu powder in MeCN solution. Dichlorophenylarsine ($PhAsCl_2$) was prepared according to literature procedure.[1]

^{1}H and ^{13}C NMR spectra were recorded using a Bruker AV-500 spectrometer at 500.13 and 125.77 MHz respectively. Chemical shifts were reported in δ (ppm) relative to $CDCl_3$.

FT-IR spectra were registered in KBr pellets on a Bruker Vertex 80 spectrometer at ambient temperature.

CHN microanalyses were performed on a MICRO cube analyzer.

Thermogravimetric analyses (TGA/c-DTA/DTG) were carried out in a closed Al_2O_3 pan under argon flow at 10 °C/min^{-1} heating rate using a NETZSCH STA 449 F1 Jupiter STA.

Powder X-ray diffraction (PXRD) patterns were recorded on a Shimadzu XRD-7000 diffractometer (Cu-Kα radiation, Ni – filter, 3–35° 2ϑ range, 0.03° 2ϑ step, 5s per point).

Steady state emission and excitation spectra were recorded on a Fluorolog 3 spectrometer (Horiba Jobin Yvon) equipped with a cooled PC177CE-010 photon detection module and an R2658 photomultiplier. The emission decays were recorded on the same instrument. The absolute PLQYs were determined at 300 K using a Fluorolog 3 Quanta-phi integrating sphere. The PLQYs at 77 K were obtained relative to those of the same samples at 300 K. Independently, the relative PLQYs were calibrated using the absolute PLQY values measured at 77 K. Temperature-dependent excitation and emission spectra as well as emission decays were recorded using an Optistat DN optical cryostat (Oxford Instruments) integrated with above spectrometer.

§2. Synthetic procedures and characterization data

Bis(2-pyridyl)phenylarsine ($AsPy_2Ph$)

Caution! These operations, which involve toxic phenyldichloroarsine ($PhAsCl_2$), must be conducted in an efficient hood!

n-BuLi (2.5 M in hexanes, 5.2 mL, 13 mmol) was added dropwise to a solution of 2-bromopyridine (2.05 g, 13 mmol) in THF (30 mL) at –78 °C, and the mixture was stirred at the same temperature for 1 h. To a resulting solution, $PhAsCl_2$ (1.45 g, 6.5 mmol) in THF (10 mL) was added dropwise at –78 °C for 10 min, and the mixture was warmed to ambient temperature and reached overnight. The reaction mixture was then quenched with water (20 mL) and extracted with CH_2Cl_2 (3 x 30 mL). The organic phases were dried over Na_2SO_4, and concentrated under reduced pressure. The residue obtained was purified through silica column chromatography (hexane:EtOAc, v/v = 1:1) to give pure product (0.378 g, 19%) as a pale solid. ^{1}H NMR (500.13 MHz, $CDCl_3$, ppm), δ: 8.73 (ddd, *J* = 4.8 Hz, *J* = 1.9 Hz, *J* = 0.9 Hz, 2H, H^6 in Py), 7.58 (dt, *J* = 7.7 Hz, *J* = 1.9 Hz, 2H, H^4 in Py), 7.52–7.49 (m, 2H, H^5 in Py), 7.40–7.35 (m, 3H, *m*-H and *p*-H in Ph), 7.32 (dt, *J* = 7.7 Hz, *J* = 1.1 Hz, 2H, *o*-H in Ph), 7.22 (ddd, *J* = 7.6 Hz, *J* = 4.9 Hz, *J* = 1.2 Hz, 2H, H^3 in Py). ^{13}C NMR (125.77 MHz, $CDCl_3$, ppm) δ: 166.6, 150.4, 139.1, 135.8, 134.4, 133.9, 128.8, 122.5. Calcd. for $C_{16}H_{13}AsN_2$ (308.21): C, 62.3; H, 4.3; N, 9.1. Found: C, 62.2; H, 4.2; N, 9.0.

*[$Cu_2(Py_2AsPh)_2Cl_2$] (**1**)*

The mixture of CuCl (12 mg, 0.12 mmol) and Py_2AsPh (37 mg, 0.12 mmol) in CH_2Cl_2 (1 mL) was stirred at room temperature for 30 min. The formed precipitate was centrifuged and dried in vacuum. White powder. Yield: 88 mg (90%). ^{1}H NMR (500.13 MHz, $CDCl_3$, ppm), δ: 9.10 (d, *J* = 5.0 Hz, 4H, H^6 in Py), 8.38 (s, 4H, H^4 in Py), 7.69–7.63 (m, 6H, *m*-H and *p*-H in Ph), 7.47 (t, *J* = 7.7 Hz, 4H, H^5 in Py), 7.17 (t, *J* = 6.4 Hz, 4H, *o*-H in Ph), 7.12 (d, *J* = 7.9 Hz, 4H, H^3 in Py). FT-IR (KBr, cm^{-1}): 415 (m), 457 (w), 478 (m), 492 (m), 615 (w), 635 (w), 671 (w), 702 (m), 758 (s), 770 (s), 988 (w), 1007 (m), 1024 (w), 1047 (w), 1082 (m), 1123 (w), 1157 (w), 1188 (w), 1233 (vw), 1275 (w), 1281 (w), 1420 (s), 1449 (vs), 1481 (w), 1537 (vw), 1558 (m), 1578 (s), 1639 (w), 1919 (vw), 2021 (vw), 2959 (w), 3032 (m), 3053 (m), 3073 (w), 3117 (vw). Calcd. for $C_{32}H_{26}As_2Cu_2Cl_2N_4$ (814.42): C, 47.2; H, 3.2; N, 6.9. Found: C, 47.1; H, 3.1; N, 6.8.

*[$Cu_2(Py_2AsPh)_2Br_2$] (**2**)*

The mixture of CuBr (12 mg, 0.083 mmol) and Py_2AsPh (26 mg, 0.084 mmol) in CH_3CN (1 mL) was stirred at room temperature for 30 min. The formed precipitate was centrifuged and dried in vacuum. White powder. Yield: 69 mg (92%). ^{1}H NMR (500.13 MHz, $CDCl_3$, ppm), δ: 9.17 (d, *J* = 5.2 Hz, 4H, H^6 in Py), 8.40 (s, 4H, H^4 in Py), 7.69–7.63 (m, 6H, *m*-H and *p*-H in Ph), 7.46 (t, *J* = 7.7 Hz, 4H, H^5 in Py), 7.16 (t, *J* = 6.4 Hz, 4H, *o*-H in Ph), 7.10 (d, *J* = 7.9 Hz, 4H, H^3 in Py). FT-IR (KBr, cm^{-1}): 415 (m), 457 (w), 476 (m), 490 (s), 617 (w), 635 (w), 669 (w), 700 (m), 733 (m), 754 (s), 768 (s), 968 (vw), 988 (w), 1005 (m), 1024 (w), 1047 (w), 1080 (m), 1121 (w), 1155 (w), 1188 (w), 1231 (vw), 1275 (w), 1281 (w), 1420 (s), 1449 (vs), 1479 (w), 1558 (m), 1578 (s), 1639 (w), 1917 (vw), 2016 (vw), 2957 (w), 3032 (m), 3051 (w), 3073 (w). Calcd. for $C_{32}H_{26}As_2Cu_2Br_2N_4$ (903.32): C, 42.5; H, 2.9; N, 6.2. Found: C, 42.5; H, 3.0; N, 6.3.

*[$Cu_2(Py_2AsPh)_2I_2$] (**3**)*

The mixture of CuI (25 mg, 0.131 mmol) and Py_2AsPh (40 mg, 0.13 mmol) in CH_3CN (1 mL) was stirred at room temperature for 30 min. The formed precipitate was centrifuged and dried in vacuum. White powder. Yield: 105 mg (81%). ^{1}H NMR (500.13 MHz, $CDCl_3$, ppm), δ: 9.24 (d, *J* = 5.1 Hz, 4H, H^6 in Py), 8.37 (s, 4H, H^4 in Py), 7.69–7.60 (m, 6H, *m*-H and *p*-H in Ph), 7.45 (dt, *J* = 7.8 Hz, *J* = 1.8 Hz, 4H, H^5 in Py), 7.15 (ddd, *J* = 7.5 Hz, *J* = 5.3 Hz, *J* = 1.3 Hz, 4H, *o*-H in Ph), 7.08 (dt, *J* = 7.9 Hz, *J* = 1.1 Hz, 4H, H^3 in Py). FT-IR (KBr, cm^{-1}): 417 (w), 461 (w), 476 (m), 486 (s), 617 (vw), 637 (w), 669 (vw), 700 (m), 745 (vs), 758 (vs), 781 (m), 964 (vw), 988 (w), 1007 (m), 1024 (w), 1049 (m), 1078 (m), 1117 (w), 1159 (m), 1186 (w), 1231 (w), 1269 (w), 1315 (w), 1410 (s), 1420 (s), 1437 (s), 1449 (vs), 1483 (w), 1558 (s), 1578 (s), 1975 (vw), 3015 (w), 3048 (m). Calcd. for $C_{32}H_{26}As_2Cu_2I_2N_4$ (997.32): C, 38.5; H, 2.6; N, 5.6. Found: C, 38.3; H, 2.6; N, 5.5.

*[$Cu_2(Py_2AsPh)_2(CH_3CN)_2](BF_4)_2$ (**4**)*

The mixture of $[Cu(CH_3CN)_4]BF_4$ (25 mg, 0.079 mmol) and Py_2AsPh (25 mg, 0.081 mmol) in CH_3CN (1 mL) was stirred at room temperature for 10 min, to the resulting solution, diethyl ether (1 mL) was then added and the precipitate formed was centrifuged and dried in vacuum. White powder. Yield: 70 mg (89%). FT-IR (KBr, cm^{-1}): 415 (w), 455 (w), 476 (w), 486 (m), 523 (w), 637 (vw), 696 (m), 746 (s), 762 (s), 770 (s), 897 (w), 972 (w), 999 (m), 1011 (s), 1040 (vs), 1059 (vs), 1157 (m), 1186 (w), 1233 (vw), 1288 (w), 1308 (w), 1371 (w), 1423 (s), 1439 (m), 1454 (s), 1483 (w), 1560 (m), 1580 (m), 1979 (vw), 2272 (w), 2307 (w), 2947 (w), 3055 (w), 3096 (w). Calcd. for $C_{36}H_{32}As_2Cu_2N_6B_2F_8$ (999.22): C, 43.3; H, 3.2; N, 8.4. Found: C, 43.2; H, 3.2; N, 8.4.

§3. Single crystal X-ray crystallography

Single crystals of **1**–**3** were grown by diffusion of Et_2O vapor into CH_3CN (for **2** and **3**) or CH_2Cl_2 (for **1**) solutions, respectively, overnight. Crystals of **4** were grown by slow evaporation of a CH_3CN solution overnight.

X-ray data and refinement details are summarized in Table S1. The data were collected on a Bruker Kappa Apex II CCD diffractometer using ϕ,ω-scans of narrow (0.5°) frames with MoKα radiation (λ = 0.71073 Å) and a graphite monochromator. The structures were solved by direct methods SHELXL97 and refined by a full matrix least-squares anisotropic-isotropic (for H atoms) procedure using SHELXL-2014/7 programs set.[1] Absorption corrections were applied using the empirical multiscan method with the SADABS program.[2] The positions of the hydrogen atoms were calculated with the riding model. Note that the crystals of **3** are prone to twinning. Therefore, the collected data for 3 were refined to take into account twinning. The refinement showed the contribution of the main twin is 0.8277(14), the second one is 0.1723(14).

Table S1. X-Ray crystallographic data for **1**–**4**.

	1	**2**	**3**	**4**
Crystal data	2090739	2090738	2090737	2095153
Chemical formula	$C_{32}H_{26}As_2Cu_2Cl_2N_4$	$C_{32}H_{26}As_2Cu_2Br_2N_4$	$C_{32}H_{26}As_2Cu_2I_2N_4$	$C_{36}H_{32}As_2Cu_2N_6{\cdot}2(BF_4)$
M_r	814.39	903.3	997.29	999.21
Crystal system, space group	Monoclinic, $P2_1/n$	Monoclinic, $P2_1/n$	Triclinic, $P1$	Monoclinic, $P2_1/n$
Temperature (K)	299	296	296	296
a, b, c (Å)	9.2247(19), 9.2436(18), 18.964(4)	9.220(3), 11.284(4), 16.043(5)	9.0573(11), 9.1282(10), 20.279(3)	8.9008(12), 9.7467(16), 22.795(4)
β(°)	99.668(9)	96.547(13)	87.224(5)	91.882(5)
V (Å^3)	1594.0(6)	1658.1(9)	1669.6(4)	1976.5(5)
Z	2	4	2	2
μ (mm^{-1})	3.59	5.70	5.12	2.81
Crystal size (mm)	0.10 × 0.10 × 0.02	0.30 × 0.05 × 0.01	0.12 × 0.10 × 0.08	0.40 × 0.30 × 0.15
T_{min}, T_{max}	0.761, 0.928	0.719, 0.928	0.695, 0.928	0.531, 0.745
No. of measured, independent and observed [$I > 2\sigma(I)$] reflections	16399, 2806, 1718	17017, 3806, 3101	15424, 5853, 4423	21894, 3401, 2305
R_{int}	0.106	0.059	0.061	0.089
$(\sin\theta/\lambda)_{max}$ (Å^{-1})	0.596	0.651	0.595	0.598
$R[F^2 > 2\sigma(F^2)]$, $wR(F^2)$, S	0.084, 0.200, 1.12	0.034, 0.089, 1.07	0.043, 0.124, 0.72	0.047, 0.114, 1.02
No. of reflections	2806	3806	5853	3401
No. of parameters	190	190	380	282
$\Delta\rho_{max}$, $\Delta\rho_{min}$ (e Å^{-3})	1.05, −0.79	0.48, −0.56	1.48, −0.95	0.44, −0.43

§4. Powder X-ray diffraction data

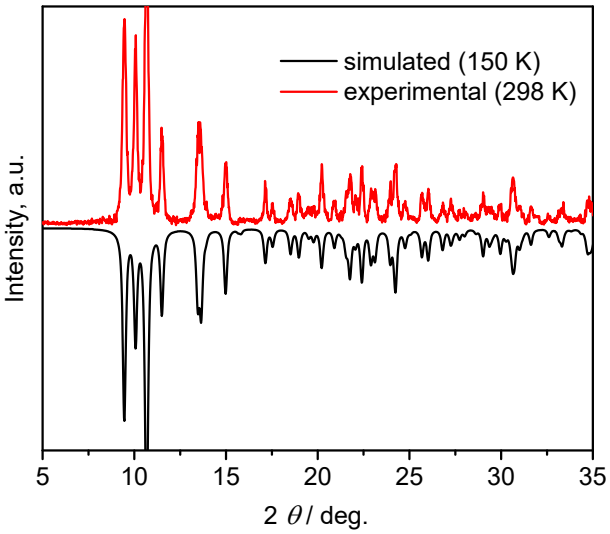

Figure S1. Experimental and simulated PXRD patterns of **1**.

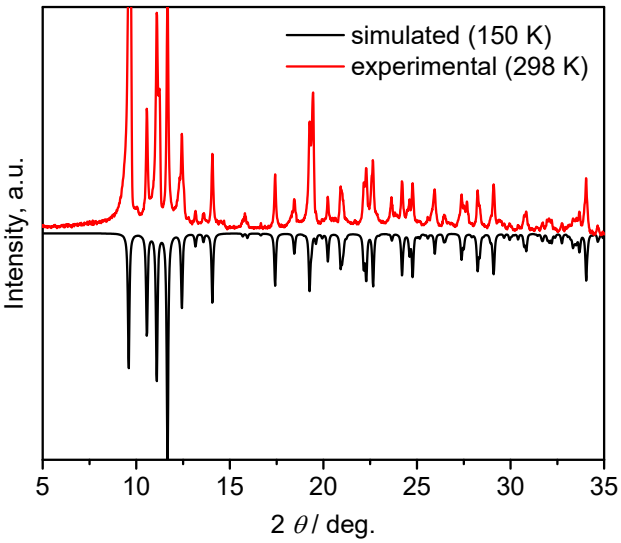

Figure S2. Experimental and simulated PXRD patterns of **2**.

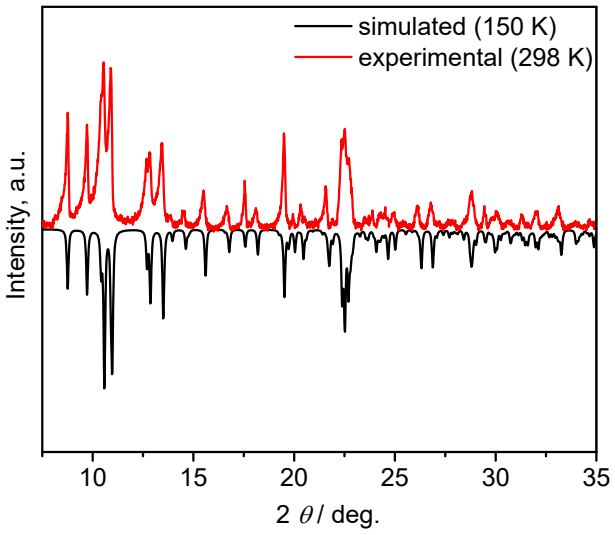

Figure S3. Experimental and simulated PXRD patterns of **3**.

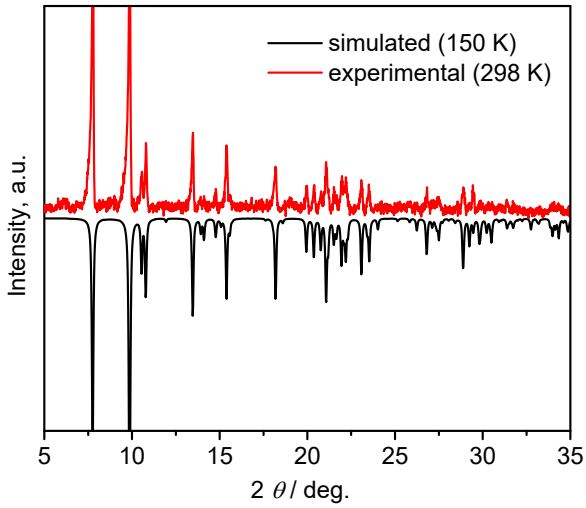

Figure S4. Experimental and simulated PXRD patterns of **4**.

§5. NMR spectra of bis(2-pyridyl)phenylarsine and complexes 1–4

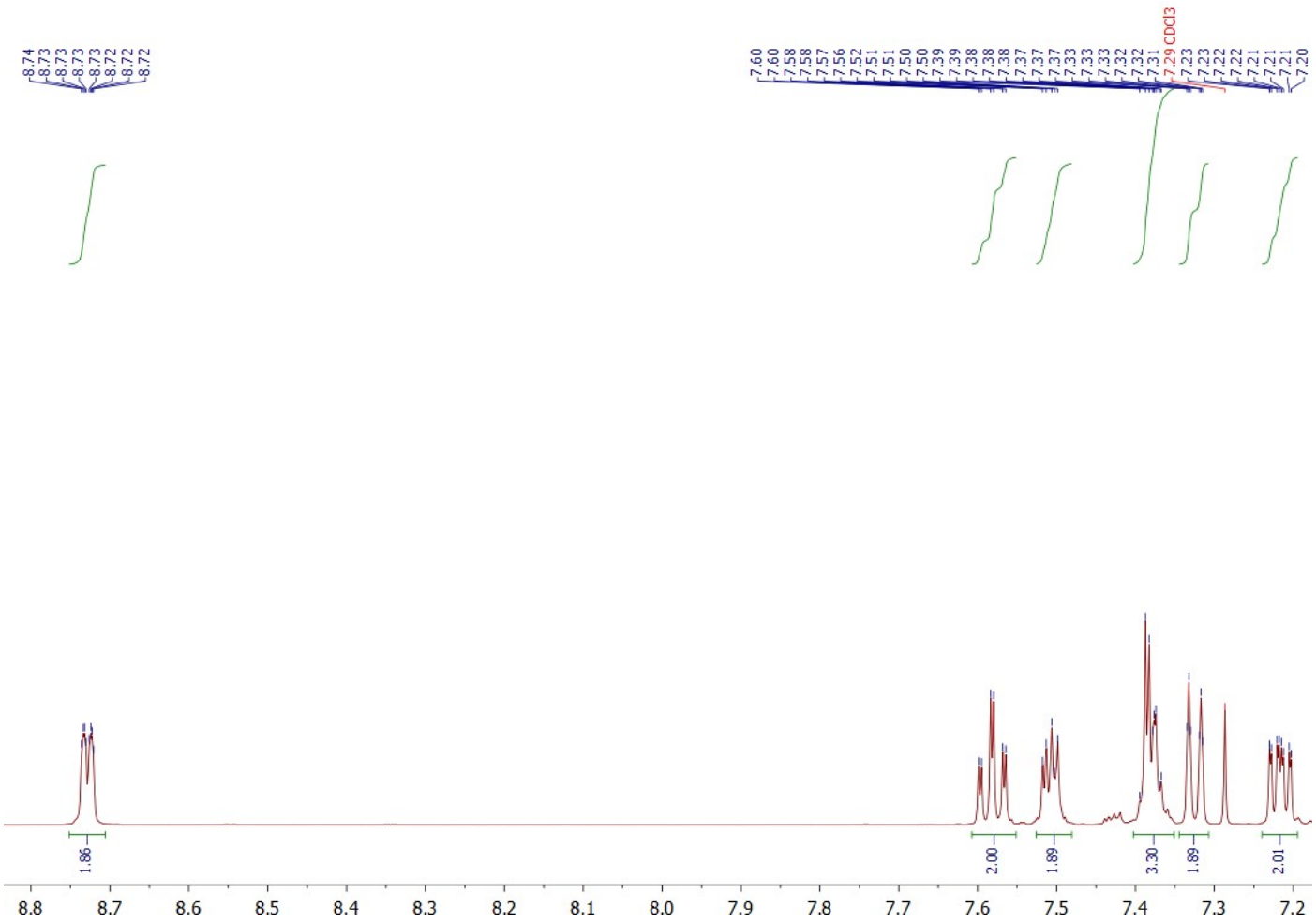

Figure S5. ^{1}H NMR spectrum of bis(2-pyridyl)phenylarsine ($CDCl_3$, 25 °C).

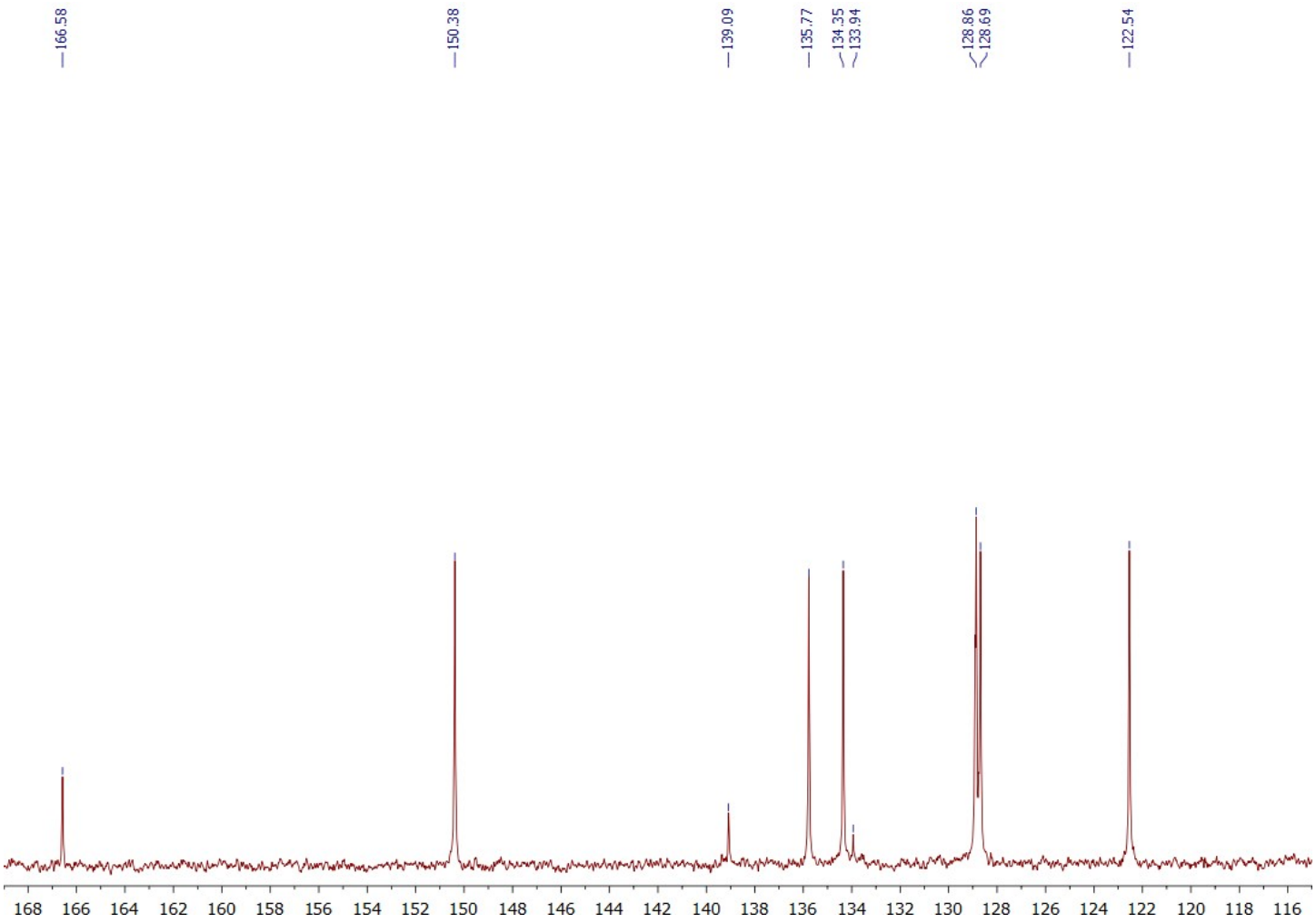

Figure S6. ^{13}C NMR spectrum of bis(2-pyridyl)phenylarsine ($CDCl_3$, 25 °C).

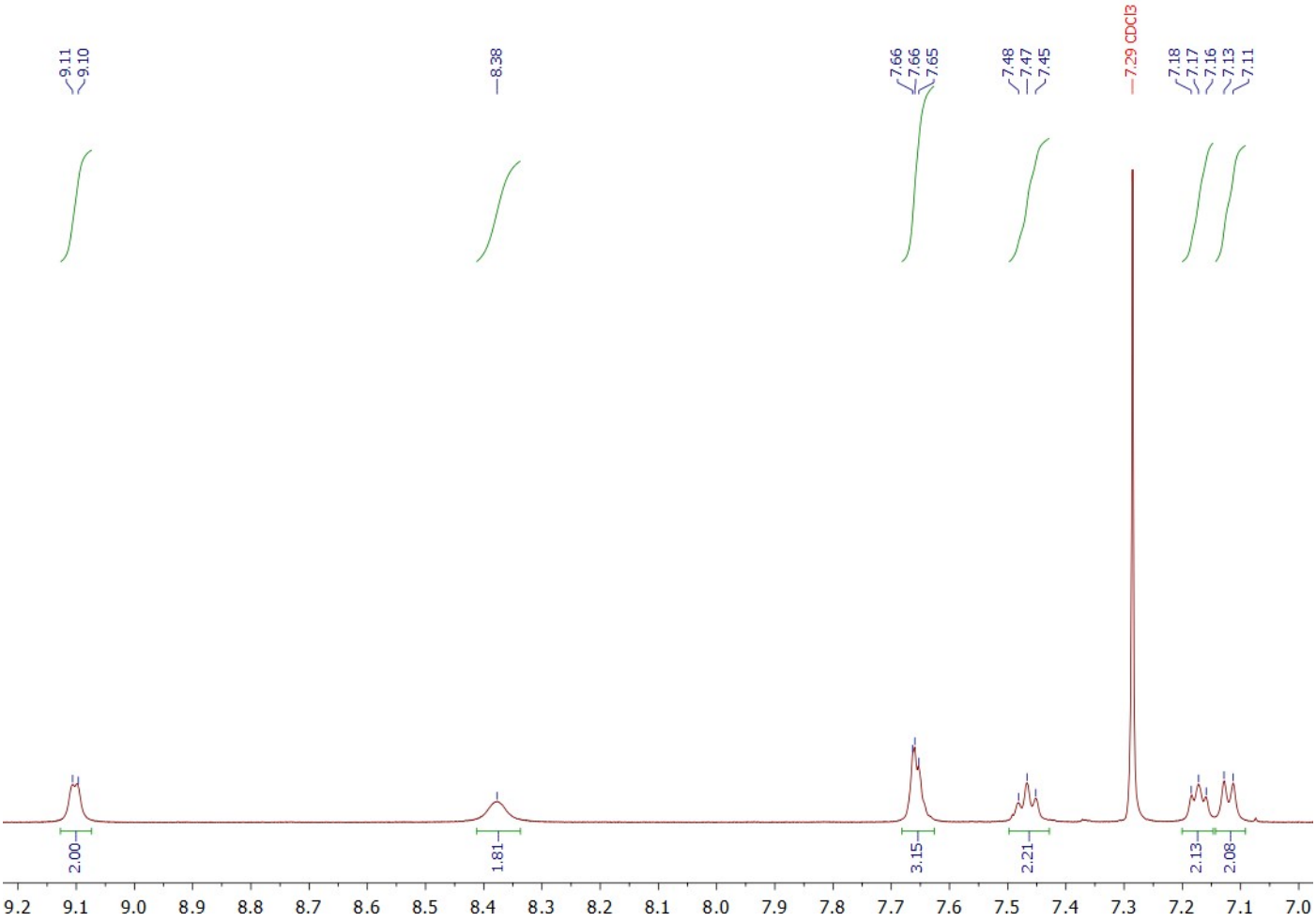

Figure S7. ^{1}H NMR spectrum of **1** ($CDCl_3$, 25 °C).

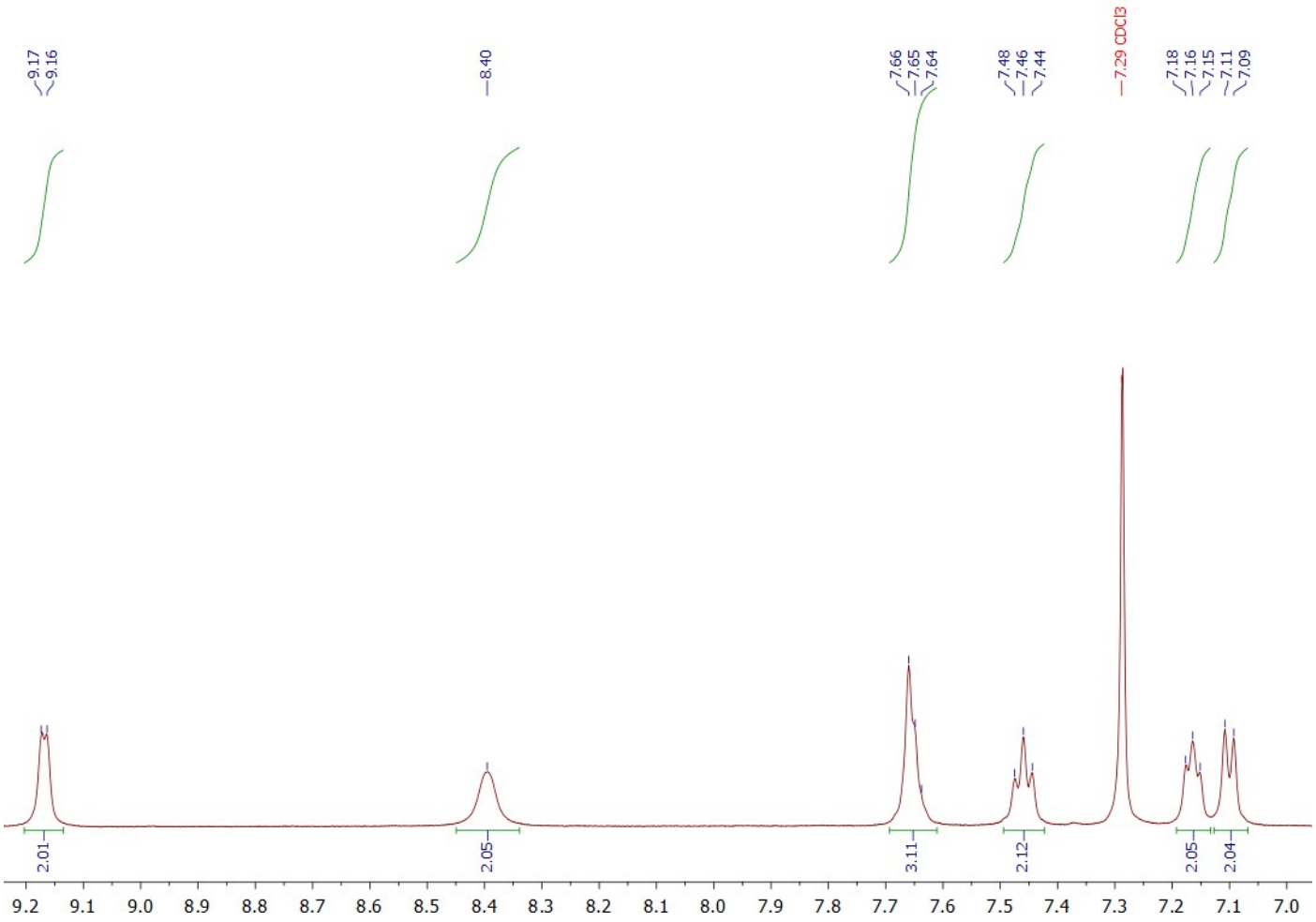

Figure S8. ^{1}H NMR spectrum of **2** ($CDCl_3$, 25 °C).

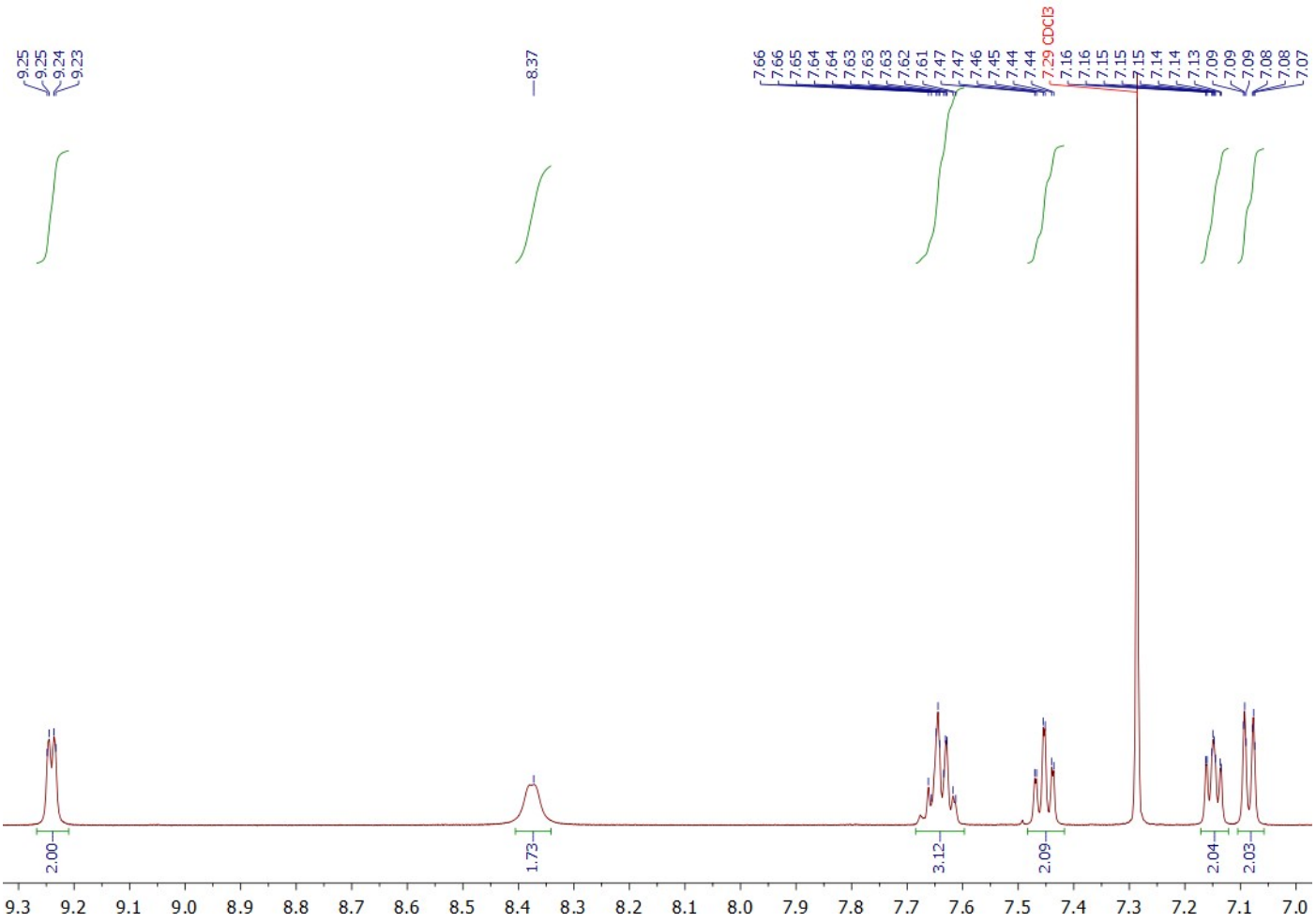

Figure S9. ^{1}H NMR spectrum of **3** ($CDCl_3$, 25 °C).

§6. FT-IR spectra

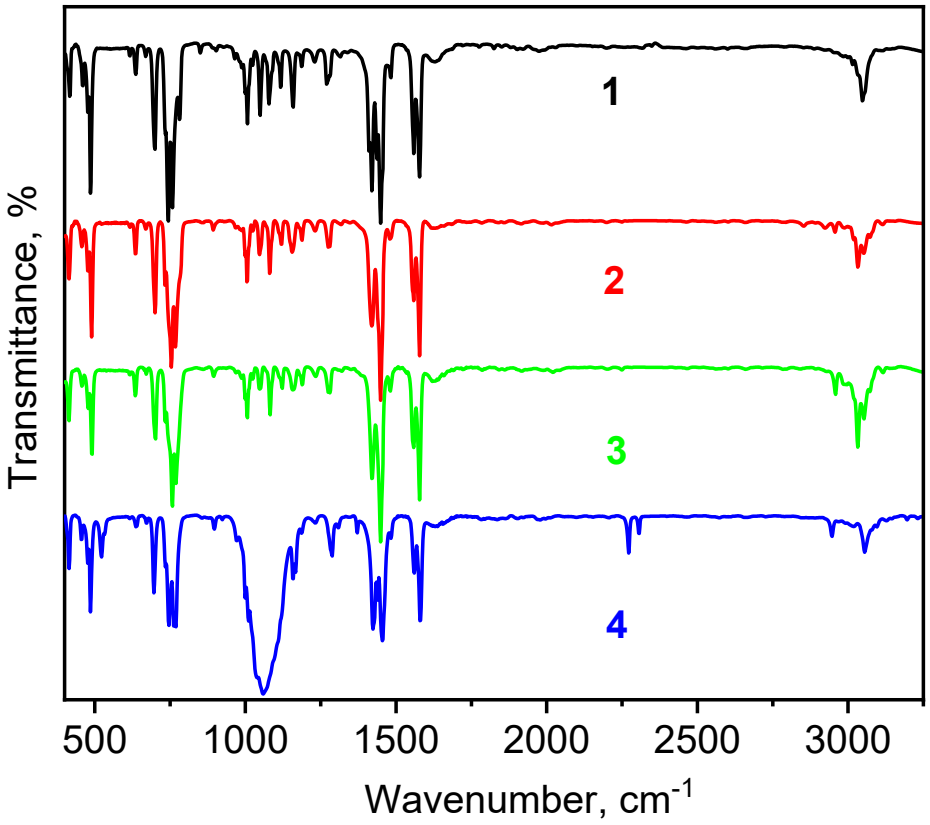

Figure S10. FT-IR spectra for the complexes **1–4** in the 500–3250 cm^{-1} region.

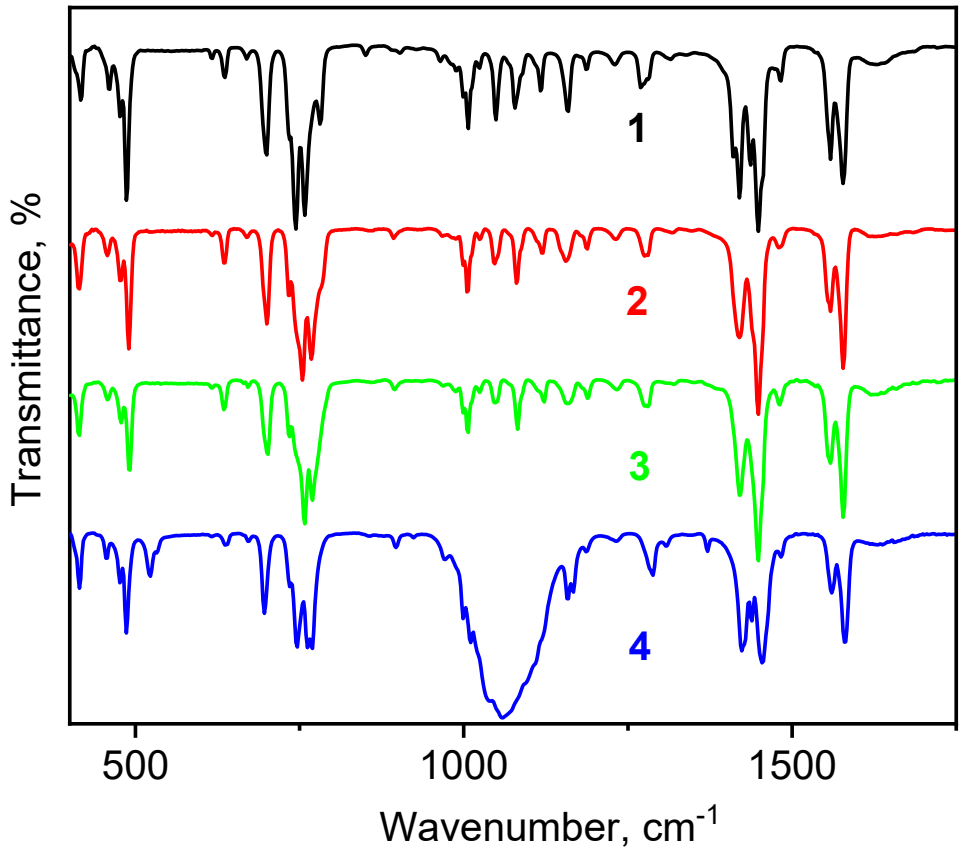

Figure S11. FT-IR spectra for the complexes **1–4** in the fingerprint region.

§7. TGA&DTG curves

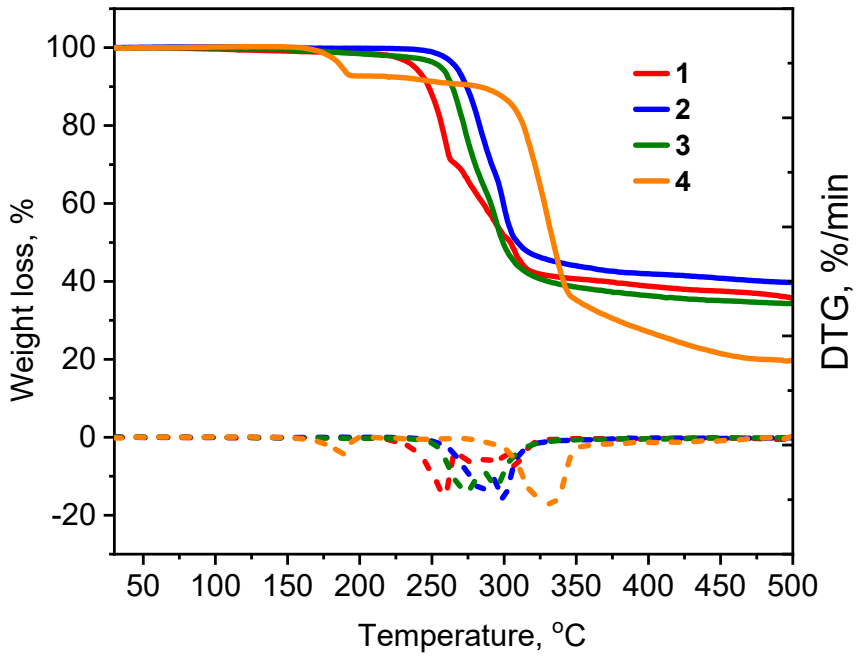

Figure S12. TGA&DTG curves for **1**–**4**.

§8. Photophysical details

To evaluate singlet-triplet splitting (ΔE_{ST}) for complexes **1**–**3**, the experimental τ_{obs}(T) dependences (Fig. 4d in main document) were fitted using Boltzmann type equation (Eq. S1) proposed for TADF model:[4]

$$\tau_{obs}(T) = (3 + \exp\left(-\frac{\Delta E_{ST}}{k_B T}\right)) \Big/ (\frac{3}{\tau_T} + \frac{1}{\tau_S} exp(-\frac{\Delta E_{ST}}{k_B T})) \qquad \text{(Eq. S1)}$$

where τ_S and τ_T are the lifetimes of the S_1 and T_1 excited states, respectively, and k_B is the Boltzmann constant. The resulting ΔE_{ST} values are outlined in Table 1 of the main document.

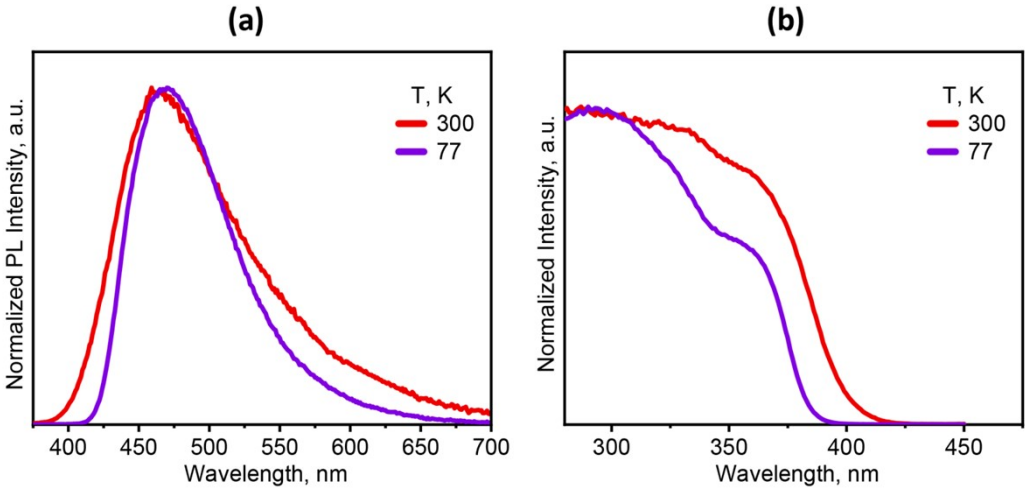

Figure S13. Emission (a) and excitation (b) spectra of **4** at 300 and 77 K. Emission spectra were recorded at λ_{ex} = 350 nm.

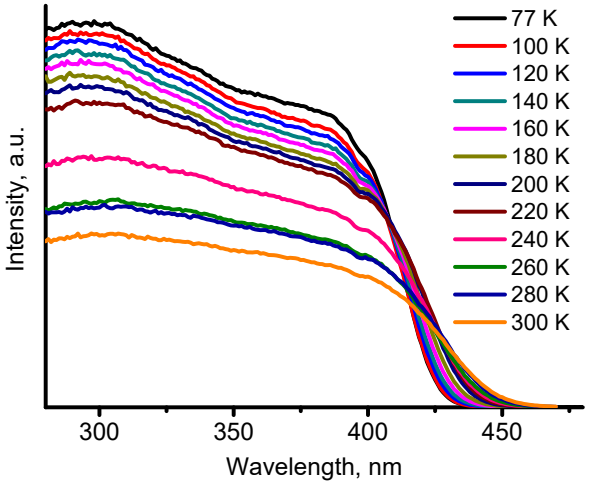

Figure S14. Temperature dependent excitation spectra of **1** (λ_{em} = 530 nm).

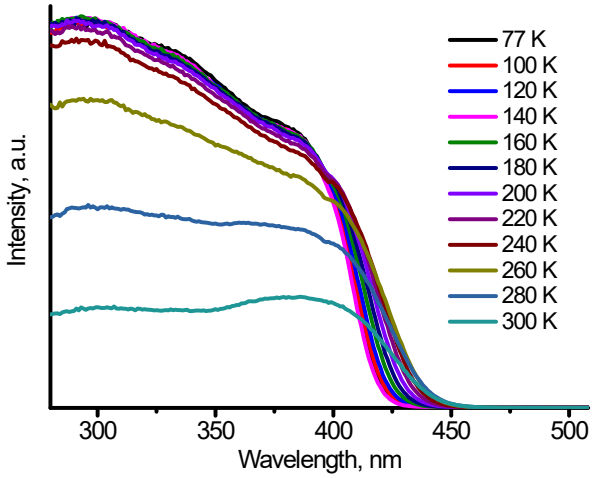

Figure S15. Temperature dependent excitation spectra of **2** (λ_{em} = 520 nm).

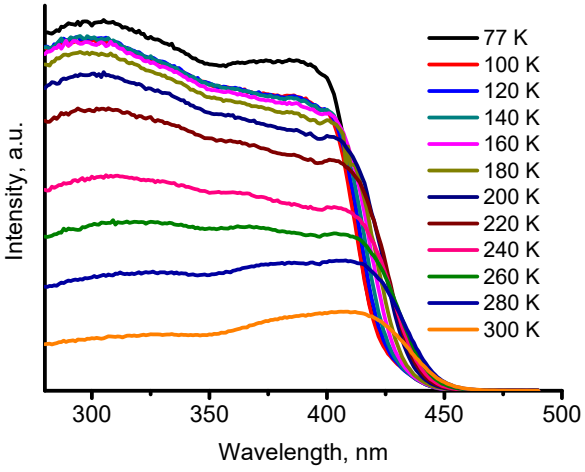

Figure S16. Temperature dependent excitation spectra of **3** (λ_{em} = 500 nm).

§9. Computational details

The DFT calculations were performed using the ADF2019[5] suite with all-electron TZ2P basis set,[6] B3LYP density functional,[7] Grimme D3BJ dispersion correction,[8] and ZORA for scalar relativistic effects.[9] Electronic excitation energies are found with Davidson's procedure for close-shell systems in a spin-restricted TDDFT calculations with scalar ZORA and no frozen core.[10]

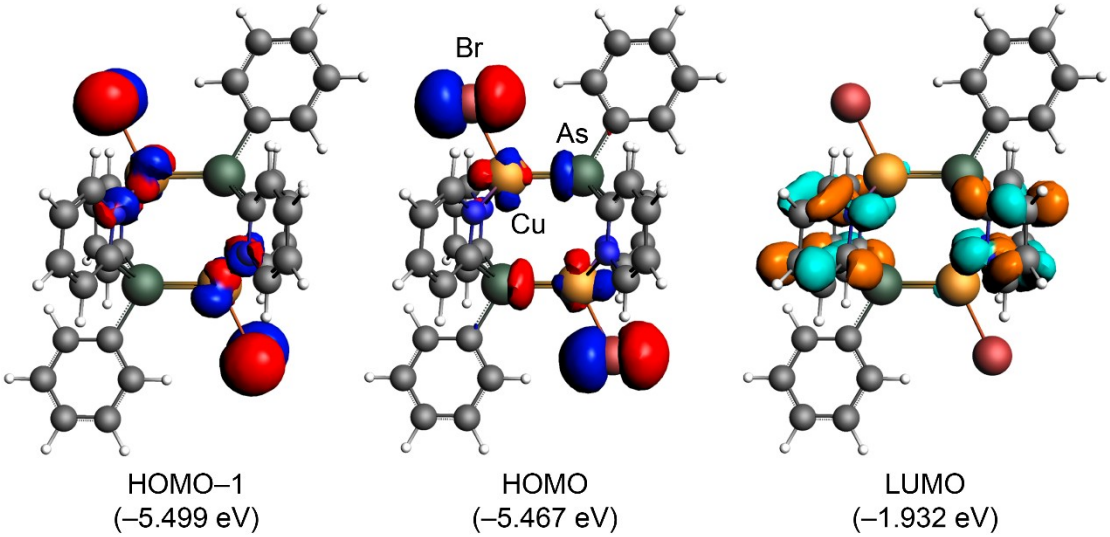

Figure S17. Frontier orbitals (isovalue of 0.03) in the ground state of $[Cu_2(Py_2AsPh)_2Br_2]$ (**2**) computed at the B3LYP/ma-ZORA-TZ2P level of theory.

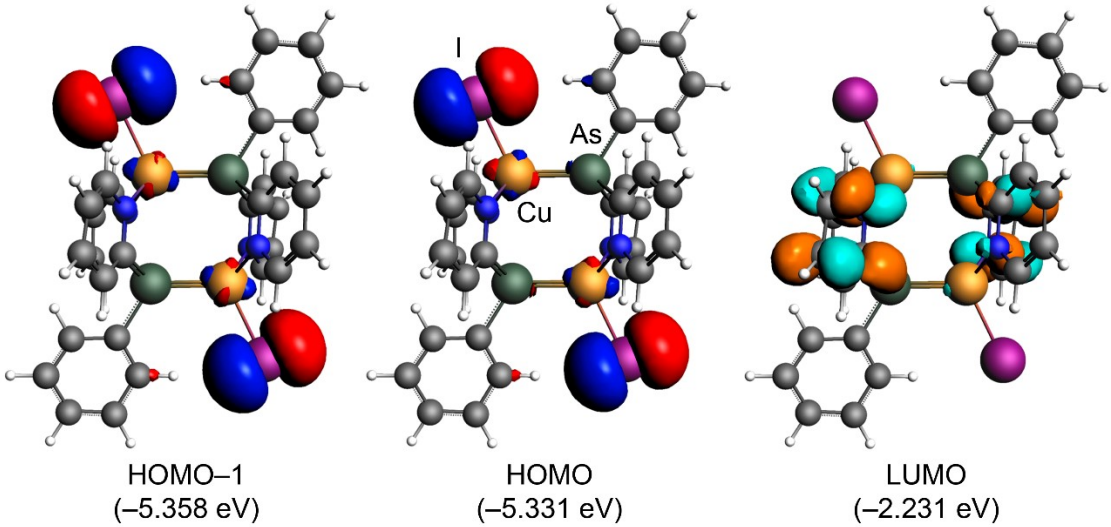

Figure S18. Frontier orbitals (isovalue of 0.03) in the ground state of $[Cu_2(Py_2AsPh)_2I_2]$ (**3**) computed at the B3LYP/ma-ZORA-TZ2P level of theory.

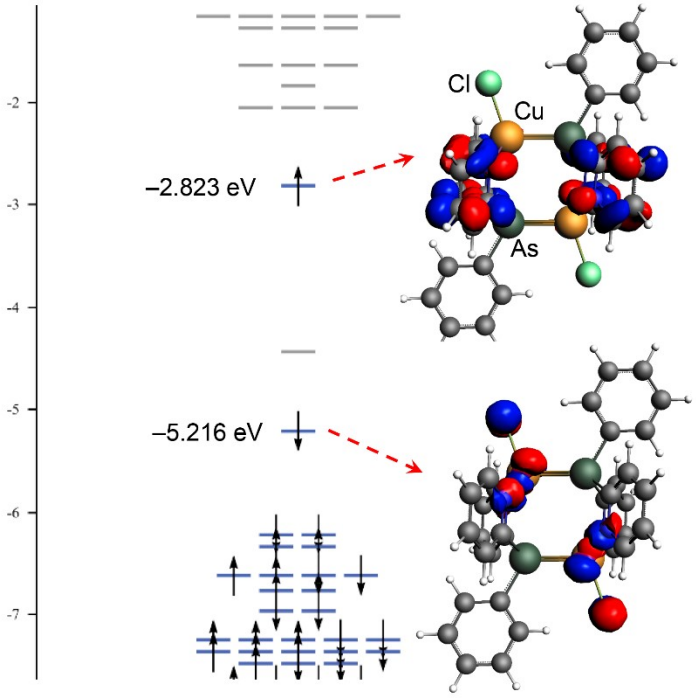

Figure S19. Single-occupied orbitals (isovalue of 0.03) in the T_1 state of $[Cu_2(Py_2AsPh)_2Cl_2]$ (**1**) computed at the B3LYP/ma-ZORA-TZ2P level of theory.

Table S2. Lowest singlet-singlet transitions (f > 0.001) in **1** calculated at TD-B3LYP-TZ2P level (gas).

λ, nm	f	Transitions (main contributions)	Character
451	0.003	HOMO → LUMO (61.4%) HOMO-1 → LUMO (23.5%)	(M+X)LCT
427	0.0014	HOMO-2 → LUMO (67.2%)	(M+X)LCT
426	0.0511	HOMO-1 → LUMO (58.0%) HOMO → LUMO (22.0%)	(M+X)LCT
418	0.0093	HOMO → LUMO+1 (42.5%) HOMO-2 → LUMO (17.4%) HOMO-1→ LUMO+1 (11.1%)	(M+X)LCT
404	0.0173	HOMO-2 → LUMO+1 (38.4%) HOMO-1 → LUMO+1(37.9%) HOMO → LUMO+1 (13.7%)	(M+X)LCT
402	0.0119	HOMO-2 → LUMO+1 (29.1%) HOMO → LUMO (22.7%) HOMO-1 → LUMO+1 (20.4%) HOMO-1→ LUMO (16.4%)	(M+X)LCT
389	0.0031	HOMO → LUMO+1 (32.8%) HOMO → LUMO (25.6%) HOMO-1 → LUMO+1 (25.6%)	(M+X)LCT
386	0.0075	HOMO-1 → LUMO+1 (31.6%) HOMO → LUMO (30.7%) HOMO → LUMO+1 (13.0%)	(M+X)LCT
383	0.0139	HOMO-1 → LUMO(55.7%) HOMO-1 → LUMO+1 (20.6%)	(M+X)LCT

		HOMO - 2 → LUMO+1 (14.0%)	
381	0.0095	HOMO → LUMO+1 (47.5%) HOMO - 1 → LUMO+1 (23.3%) HOMO - 2 → LUMO (10.2%)	(M+X)LCT
370	0.0016	HOMO-2 → LUMO (78.3%)	(M+X)LCT
368	0.0016	HOMO → LUMO+2 (44.7%) HOMO - 2 → LUMO+1 (24.3%) HOMO - 1 → LUMO+2 (13.0%)	(M+X)LCT
367	0.0083	HOMO - 2 → LUMO+1 (60.5%) HOMO → LUMO+2 (18.8%) HOMO - 2 → LUMO (7.1%)	(M+X)LCT

Table S3. Lowest singlet-singlet transitions (f > 0.0001) in **2** calculated at TD-B3LYP-TZ2P level (gas).

λ, nm	f	Transitions (main contributions)	Character
445	0.0013	82.9% HOMO-1 → LUMO 9.8% HOMO-1 → LUMO+1	(M+X)LCT
427	0.0438	75.0% HOMO → LUMO 11.5% HOMO-1 → LUMO+1	(M+X)LCT
388	0.0073	34.5% HOMO-1 → LUMO+1 31.4% HOMO-2 → LUMO 16.1% HOMO → LUMO	(M+X)LCT
419	0.0008	53.7% HOMO-2 → LUMO 27.7% HOMO-1 → LUMO+1	(M+X)LCT
411	0.0299	76.1% HOMO → LUMO+1 16.0% HOMO → LUMO	(M+X)LCT
405	0.0021	68.5% HOMO-2 → LUMO+1 21.8% HOMO → LUMO	(M+X)LCT
391	0.0062	56.5% HOMO → LUMO 16.9% HOMO → LUMO+1 16.7% HOMO-2 → LUMO+1	(M+X)LCT
387	0.0056	69.8% HOMO-1 → LUMO 16.2% HOMO-1 → LUMO+1	(M+X)LCT
384	0.0021	77.4% HOMO-1 → LUMO+1 8.1% HOMO-1 →LUMO	(M+X)LCT
382	0.0111	74.1% HOMO → LUMO+1 7.3% HOMO-2 → LUMO	(M+X)LCT
372	0.0004	86.2% HOMO-2 → LUMO 9.4% HOMO-2 → LUMO+1	(M+X)LCT
366	0.0077	90.5% HOMO-2 → LUMO+1	(M+X)LCT
365	0.0014	76.7% HOMO-1 → LUMO+2	(M+X)LCT

Table S4. Lowest singlet-singlet transitions (f > 0.0001) in **3** calculated at TD-B3LYP-TZ2P level (gas).

λ, nm	f	Transitions (main contributions)	Character
500	0.0017	73.3% HOMO-1 → LUMO 9.7% HOMO → LUMO	(M+X)LCT
491	0.0189	80.0% HOMO → LUMO	(M+X)LCT

		10.9% HOMO-1 → LUMO	
463	0.011	77.7% HOMO-2 → LUMO 7.0% HOMO-1 → LUMO+1	(M+X)LCT
458	0.0061	39.4% HOMO-1 → LUMO 19.7% HOMO → LUMO+1 11.3% HOMO-1 → LUMO	(M+X)LCT
454	0.0045	35.3% HOMO → LUMO 27.1% HOMO → LUMO+1 16.3% HOMO-1 → LUMO+1	(M+X)LCT
445	0.0112	44.1% HOMO → LUMO 37.0% HOMO → LUMO+1	(M+X)LCT
439	0.0024	65.6% HOMO-1 → LUMO 14.0% HOMO-1 → LUMO+1	(M+X)LCT
427	0.0127	57.2% HOMO-2 → LUMO+1 23.9% HOMO → LUMO+1	(M+X)LCT
422	0.0062	56.3% HOMO → LUMO+1 17.7% HOMO-2 → LUMO+1 10.7% HOMO-2 → LUMO	(M+X)LCT
415	0.0004	75.0% HOMO-1 → LUMO+1 15.5% HOMO-1 → LUMO+1	(M+X)LCT
410	0.0096	75.3% HOMO-2 → LUMO 14.9% HOMO-2 → LUMO+1	(M+X)LCT
402	0.0049	84.5% HOMO-3 → LUMO	(M+X)LCT
389	0.0127	88.9% HOMO-2 → LUMO+1	(M+X)LCT

§10. References

[1] R. Betz, M.M. Reichvilser, E. Schumi, C. Miller, P. Klüfers, *ZAAC,* **2009**, *635*, 1204.

[2] G.M. Sheldrick, *Acta Crystallogr., Sect. C: Struct. Chem*., **2015**, *71*, 3.

[3] *SADABS*, v. 2008-1, Bruker AXS, Madison, WI, USA, 2008.

[4] *Highly Efficient OLEDs Materials Based on Thermally Activated Delayed Fluorescence*, Ed. Yersin, H.; Wiley-VCH, Weinheim, 2019.

[5] G. te Velde, F.M. Bickelhaupt, E.J. Baerends, C. Fonseca Guerra, S.J.A. van Gisbergen, J.G. Snijders, T. Ziegler, *J. Comput. Chem*., **2001**, *22*, 931.

[6] E. van Lenthe, E.J. Baerends, *J. Comput. Chem*., **2003**, *24*, 1142.

[7] P.J. Stephens, F.J. Devlin, C.F. Chabalowski, M.J. Frisch, *J. Phys. Chem*., **1994**, *98*, 11623.

[8] S. Grimme, S. Ehrlich, L. Goerigk, *J. Comput. Chem*., **2011**, *32*, 1457.

[9] E. van Lenthe, A.E. Ehlers, E.J. Baerends, *J. Chem. Phys*., **1999**, *110*, 8943.

[10] S.J.A. van Gisbergen, J.G. Snijders, E.J. Baerends, *Comput. Phys. Commun*., **1999**, *118*, 119.